*DOI:*
10.1073/pnas.1324118111

*Document Version*
Publisher's PDF, also known as Version of record

# Rich-club organization of the newborn human brain

Gareth Ball[a], Paul Aljabar[a,1], Sally Zebari[a], Nora Tusor[a], Tomoki Arichi[a], Nazakat Merchant[a], Emma C. Robinson[b], Enitan Ogundipe[c], Daniel Rueckert[d], A. David Edwards[a,2], and Serena J. Counsell[a,2]

[a]Centre for the Developing Brain, Division of Imaging Sciences and Bioengineering, King's College London, King's Health Partners, St Thomas' Hospital, London SE1 7EH, United Kingdom; [b]Functional Magnetic Resonance Imaging of the Brain Group, Nuffield Department of Clinical Neuroscience, University of Oxford, Oxford OX3 9DU, United Kingdom; [c]Department of Paediatrics, Chelsea and Westminster Hospital, Imperial College London, London SW10 9NH, United Kingdom; and [d]Biomedical Image Analysis Group, Department of Computing, Imperial College London, London SW7 2AZ, United Kingdom

Edited by Marcus E. Raichle, Washington University in St. Louis, St. Louis, MO, and approved April 7, 2014 (received for review January 1, 2014)

**Combining diffusion magnetic resonance imaging and network analysis in the adult human brain has identified a set of highly connected cortical hubs that form a "rich club"—a high-cost, high-capacity backbone thought to enable efficient network communication. Rich-club architecture appears to be a persistent feature of the mature mammalian brain, but it is not known when this structure emerges during human development. In this longitudinal study we chart the emergence of structural organization in mid to late gestation. We demonstrate that a rich club of interconnected cortical hubs is already present by 30 wk gestation. Subsequently, until the time of normal birth, the principal development is a proliferation of connections between core hubs and the rest of the brain. We also consider the impact of environmental factors on early network development, and compare term-born neonates to preterm infants at term-equivalent age. Though rich-club organization remains intact following premature birth, we reveal significant disruptions in both in cortical–subcortical connectivity and short-distance corticocortical connections. Rich club organization is present well before the normal time of birth and may provide the fundamental structural architecture for the subsequent emergence of complex neurological functions. Premature exposure to the extrauterine environment is associated with altered network architecture and reduced network capacity, which may in part account for the high prevalence of cognitive problems in preterm infants.**

connectome | brain development | tractography | preterm birth

To understand the functional properties of a complex network it is necessary to examine its structural organization and topological properties. In the human brain this can be achieved at a macroscale by tracing white matter connections between brain regions with diffusion MRI; this enables the interrogation of structural network topology in vivo with millimeter-scale spatial resolution, providing complementary evidence to experimental studies (1, 2).

Network analysis of the adult human structural connectome has revealed a set of highly connected cortical "hubs" predominantly located in heteromodal association cortex, that provide a foundation for coherent neuronal activation across distal cortical regions (3–5). Further, some hub regions tend to be densely connected to each other, forming a "rich club" comprised of frontal and parietal cortex, precuneus, cingulate and the insula, as well as the hippocampus, thalamus, and putamen (6). Rich-club organization has been identified in a number of complex networks (7) and represents an attractive feature for investigation in the brain because rich-club connections tend to dominate network topology (8). Rich-club architecture appears to be a fundamental feature of the mature mammalian brain with similar organization identified in animal models (9, 10).

It has been suggested that the emergence of complex neurological function is associated with the integration of major hubs across the cortex (11, 12), and that the neural connectivity underlying this undergoes substantial remodeling after birth (13, 14). Initial studies of neonatal structural networks have reported only dense local connectivity within segregated modules and few long-distance connections (12, 15). In contrast, functional MRI reveals large-scale dynamic functional networks analogous to those seen in adults (16, 17) and compatible with more advanced cerebral maturation. To address the possibility that the newborn brain may be structurally more developed than previously thought, and to understand better the role of structural network architecture in emergent neurological functions, we have developed an approach to assess the topological development of structural connectivity in the human brain up to the normal time of birth.

We used this approach to define network topology at ∼30 and 40 wk of gestation and, in a group of infants studied at both time points, charted the emergence of structural organization. We also explored the specific relations of cortical and deep gray matter hubs in the network. To determine whether network development was independent of environmental factors, we compared healthy term-born subjects with infants prematurely born and exposed to the extrauterine environment. We report that highly ordered cerebral structural connectivity with rich club topology is established by 30 wk gestation; additionally, we identify aspects of network organization that develop during this period and specific features that are disturbed by premature extrauterine life.

## Results

**Rich-Club Organization of the Newborn Brain.** As an initial examination of connectivity in the developing brain, datasets were grouped according to age at scan: early (median age at scan = $31^{+1}$ weeks; 28 preterm infants) and term (median age at scan = $41^{+2}$ weeks; 46 preterm infants and 17 term-born controls).

At the early, 30-wk time point, average node degree was lower, but both time points had similar asymmetric and heavy-tailed degree distributions (Fig. 1 *A* and *B*) that follow an exponentially truncated power law [$p(k) = k^{a-1} \cdot e^{k/k_c}$; Fig. 1*B*, *Inset*],

### Significance

To investigate the organizational principles of human brain development, we analyzed cerebral structural connectivity in the period leading up to the time of normal birth. We found that a "rich club" of interconnected cortical hubs previously reported in adults is present by 30 wk gestation. From mid to late gestation, connections between core hubs and the rest of the brain increased significantly. To determine the influence of environmental factors on network development, we also compared term-born infants to those born prematurely. Alterations in cortical–subcortical connectivity and short-distance connections outside the core network were associated with prematurity. Rich-club organization in the human brain precedes the emergence of complex neurological function, and alterations during this time may impact negatively on subsequent neurodevelopment.

Author contributions: G.B., A.D.E., and S.J.C. designed research; G.B., P.A., N.T., T.A., N.M., and E.O. performed research; G.B., P.A., E.C.R., and D.R. contributed new reagents/analytic tools; G.B. and S.Z. analyzed data; and G.B., P.A., A.D.E., and S.J.C. wrote the paper.

The authors declare no conflict of interest.

This article is a PNAS Direct Submission.

Freely available online through the PNAS open access option.

[1]To whom correspondence should be addressed. E-mail: paul.aljabar@kcl.ac.uk.

[2]A.D.E. and S.J.C. contributed equally to this work.

This article contains supporting information online at www.pnas.org/lookup/suppl/doi:10.1073/pnas.1324118111/-/DCSupplemental.

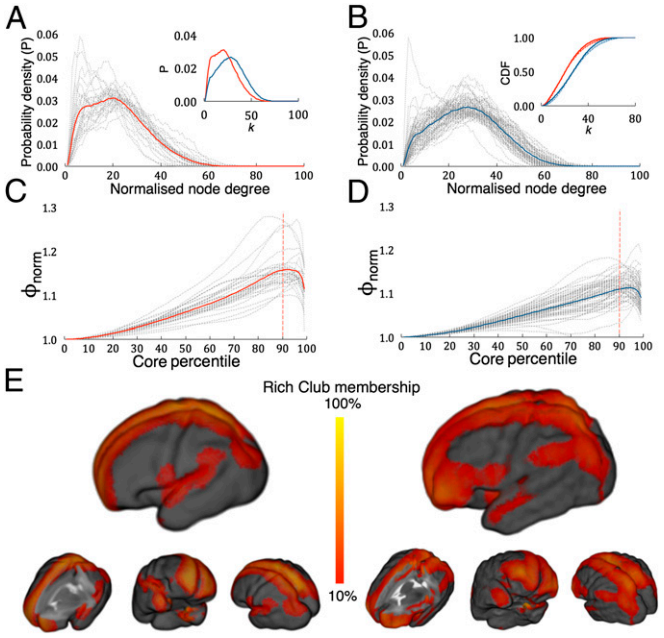


**Fig. 1.** Structural organization of the developing human brain. Mean degree distribution, normalized by the number of nodes in each network, at 30 wk (*A*, red solid line) and 40 wk (*B*, blue line), overlaid on individual distributions (dashed lines; $n$ = 28 and 63, respectively). (*A*, *Inset*) Distributions at both time points. (*B*, *Inset*) Cumulative distribution plots (solid lines) and power law fits (dashed lines). (*C* and *D*) Mean normalized rich-club curves ($\Phi_{norm}$) and individual curves (30 wk, *C*; 40 wk, *D*). The red dashed line indicates the $RC_{90}$ rich-club threshold. (*E*) Maps at both time points showing the membership probabilities of regions belonging to the $RC_{90}$ network.

suggesting broad-scale network characteristics and the presence of a set of highly connected hubs (18, 19).

Rich-club organization was evident at both time points (Fig. 1 *C* and *D*), with the normalized rich-club coefficient, $\phi_{norm}$, peaking for most subjects when core networks contained the top 10% of nodes by degree and above (peak $\phi_{norm}$: early = 1.16, core = 91%; term = 1.11, core = 95%). The top 10% nodes (Fig. 1 *C* and *D*, red dashed line) were chosen to represent the rich club, designated $RC_{90}$. This nominal threshold for the highest-degree nodes in each network ensures equal numbers of nodes are used to construct rich-club maps, regardless of average degree across subjects. Rich-club maps were averaged to create a voxel-wise probability map of $RC_{90}$ membership for group comparison (Fig. 1*E*).

A cortical network of high-degree hubs was identified at both time points (Fig. 1 and Movies S1 and S2), including medial frontal and superior parietal cortex, supplementary motor areas, the precuneus and paracentral lobule, hippocampi, and, additionally, the insula and inferior frontal cortex at 40 wk [cortical regions identified using the automated anatomical labeling (AAL) neonatal atlas (20); for details, see Table S1].

**Longitudinal Development of the Rich Club.** Network topology and connectivity within and between core rich-club nodes and peripheral, low-degree nodes were examined in a longitudinal dataset of 28 infants scanned twice during the preterm period at 30 and 40 wk.

Network topology was summarized by averaging density, mean clustering coefficient ($C$) and characteristic path length ($L$) over 100 networks for each subject (Fig. S1*D*). At 30 wk, density = 0.22 ± 0.04 (mean ± SD), $C$ = 0.64 ± 0.03, and $L$ = 1.88 ± 0.10. By 40 wk, density = 0.29 ± 0.04, $C$ = 0.66 ± 0.02, and $L$ = 1.77 ± 0.06. After comparison with a set of randomized networks, normalized $C$ and $L$ metrics, $C_{norm}$ and $L_{norm}$ were found to significantly decrease over the preterm period ($n$ = 28; paired $t$ test: $P < 0.001$ both).

Network connectivity was examined by distinguishing different types of connections: local connections between peripheral nodes; feeder connections between peripheral and core nodes; and core connections between core nodes only (21). The degree for an individual node can be separated into components according to its connections (core, feeder, or local). Fig. 2 shows the average degree of core nodes in these components. Degree based on all connections is shown in Fig. 2*A*. Fig. 2*B* restricts the degree count to feeder connections, and Fig. 2*C* considers only core connections. In each case, we vary the definition of the core by adjusting the threshold for core membership (as a percentile of maximum degree), and the effect of this variation on the average core node's degree is plotted. At low percentiles, the network core contains most of the nodes, whereas at higher levels, only the most connected, topologically dominant nodes (i.e., the rich club) form the core.

By 40 wk, average degree of core nodes was significantly higher [repeated-measures ANOVA: $F_{(1,99)}$ = 67.0, $P < 0.001$]. There was a significant increase in both the average number of feeder connections (Fig. 2*B*) and the number of local connections between excluded peripheral nodes ($F$ = 57.8, 69.1, $P <$ 0.001 both). Average within-core node degree (core connections only), normalized to the number of nodes in the core network, increased over time ($F$ = 42.2, $P < 0.001$), but a significant group × core-threshold interaction ($F$ = 87.2, $P < 0.001$) and post hoc $t$ tests revealed that there was no significant increase in core network degree within the peak rich-club domain. In

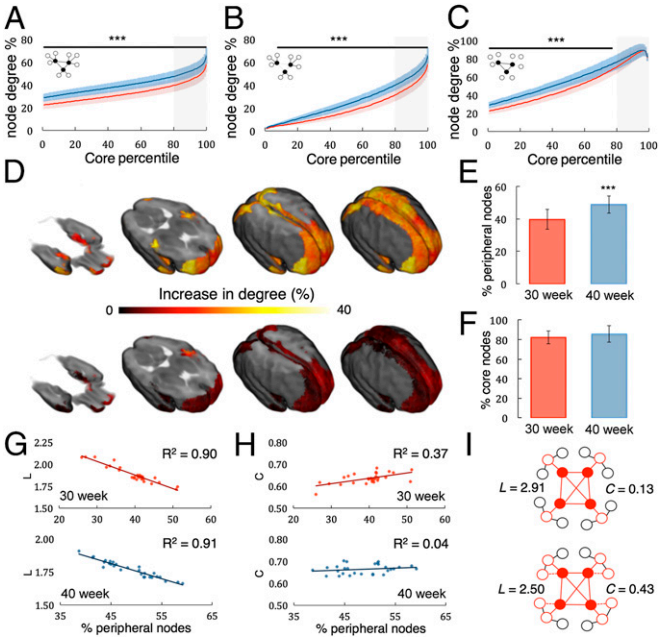


**Fig. 2.** Rich-club organization during the preterm period. Average node degree of core nodes by connection type: (*A*) all connections, (*B*) feeder connections, and (*C*) core connections (normalized by the total number of nodes, number of peripheral nodes, and number of core nodes, respectively). Data show group mean at the 30-wk (red) and 40-wk (blue) time points ($n$ = 28; shading indicates SD). Significant differences are shown with a black bar (post hoc paired $t$ tests: $P < 0.001$). Gray shading represents the peak rich-club domain. Schematics show connections of interest in each plot. (*D*) Mean percent increase in node degree due to feeder connections (*Upper*) and core connections (*Lower*) in $RC_{90}$ nodes are compared in *E* and *F*. Feeder connectivity of $RC_{90}$ nodes is related to global network metrics *L* (characteristic path length) and *C* (clustering coefficient) at both time points (*G* and *H*). Developmental changes in rich-club connectivity are illustrated in *I* (filled circles are core nodes); adding feeder connections decreases *L* and increases *C*.

the $RC_{90}$ network, a significant increase in the number of feeder connections was evident over the preterm period (Fig. 2*E*), but there was no significant increase in the number of core connections (Fig. 2*F*). Feeder connectivity within the $RC_{90}$ network was significantly associated with decreasing $L$ at both time points (Fig. 2*G*; 30 wk: $R^2 = 0.90$; 40 wk: $R^2 = 0.91$, $P < 0.001$ both), whereas $C$ was found to be significantly associated with feeder connectivity at the 30-wk time point only (Fig. 2*H*; 30 wk: $R^2 = 0.37$, $P < 0.001$; 40 wk: $R^2 = 0.04$, $P = 0.29$).

Fig. 2*I* illustrates these changes using a simple representative network. The addition of four feeder connections (dashed red lines), representing an increase in connectivity between high-degree core nodes and low-degree peripheral nodes, decreases path length by 14% while the clustering coefficient rises; reflected in the absolute (nonnormalized) values of $C$ observed at the early and term time points (30 wk: mean ± SD = 0.64 ± 0.03; 40 wk: 0.66 ± 0.02; $P < 0.001$).

**Rich-Club Organization and Prematurity.** Structural connectivity and network topology was compared at term in all infants born preterm ($n = 46$) and a cohort of term-born controls ($n = 17$). No significant differences were found in mean network density (preterm: 0.28 ± 0.04; term: 0.28 ± 0.03, $P = 0.80$) or path length $L$ (Fig. 3*D*; preterm: $L = 1.78 \pm 0.07$; term = 1.76 ± 0.05, $P = 0.25$). After normalization, a small increase in $L_{norm}$ was apparent in the preterm infants (Fig. 3*D*; $P < 0.05$). In contrast, $C$ was significantly greater in the preterm cohort both before (Fig. 3*D*; preterm: $C = 0.66 \pm 0.02$; term: $C = 0.64 \pm 0.02$, $P < 0.01$) and after normalization (Fig. 3*D*; $P < 0.001$). Voxel-wise comparison revealed significantly higher clustering in preterm infants in the lateral parietal cortex, ventral and lateral frontal cortex, and around the Sylvian fissure (Fig. 3*E*; $P < 0.01$, family-wise error corrected after threshold-free cluster enhancement) (22).

No significant differences were found between groups in core network node degree when considering all connections [Fig. 3*A*; $F_{(1,99)} = 0.77$, $P = 0.38$], feeder connections (Fig. 3*B*; $F = 0.25$, $P = 0.62$), or core connections (Fig. 3*C*; $F = 1.76$, $P = 0.19$). However, a significant group × core threshold interaction ($F = 2.87$, $P < 0.001$) and post hoc $t$ tests revealed a significant increase in local connections between peripheral nodes at lower core network thresholds in the preterm cohort (Fig. 3*F*; $P < 0.01$). Exploring the influence of peripheral connectivity on network topology, linear regression also revealed that the number of local connections between the lowest ranked 10% of nodes was significantly associated with $C$ ($R^2 = 0.46$, $P < 0.001$). Fig. 3*G* illustrates an increase in peripheral connectivity in a simple network. The addition of a small number of local connections significantly increases $C$ but has little effect on $L$.

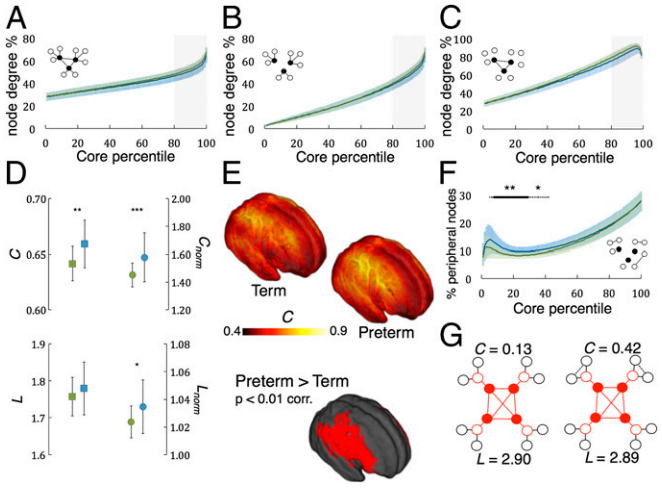


**Fig. 3.** Rich-club organization at term-equivalent age. Average node degree of core nodes based on connection type (*A*) all connections, (*B*) feeder connections, and (*C*) core connections (normalized by the total number of nodes, number of peripheral nodes, and number of core nodes, respectively). Data show group mean of preterm infants at term-equivalent age (blue) and term-born controls (green) (shading indicates SD). Gray shading represents rich-club domain. (*D*) Mean clustering coefficient, $C$, and average path length, $L$, for each group (squares; preterm, blue; term, green), circles show normalized values ($C_{norm}$ and $L_{norm}$; error bars show SD; $^*P < 0.05$, $^{**}P < 0.01$, $^{***}P < 0.001$ $t$ test). (*E*) Group mean maps of the clustering coefficient $C$. Regions where $C$ was significantly higher in the preterm group are shown below (general linear model: 5,000 permutations, $P < 0.01$ corrected). (*F*) Local connections of peripheral nodes with a varying threshold for core membership. Significant differences are shown with dashed ($^*P < 0.05$) and solid ($^{**}P < 0.01$) black lines. The illustrative network (*G*) shows that increasing the number of edges between peripheral nodes (dashed black lines) increases $C$ but does not affect $L$.

**Exploring Connectivity Within the Rich Club.** In the adult, connections linking rich-club nodes are physically longer than those connecting non–rich-club nodes, forming a high-cost backbone (21). By calculating the Euclidean distance between pairs of connected nodes we confirmed that, in all three groups, core connections of the $RC_{90}$ networks were significantly longer than both feeder and local connections ($P < 0.001$ all; Fig. S2).

The adult rich club consists of several cortical hubs alongside deep gray-matter structures, including the thalamus and putamen (6). To explore the influence of deep gray-matter pathways on rich-club organization, whole-brain tractography was repeated excluding all streamlines passing through deep gray matter. Retaining only edges that connected two cortical regions of interest (ROI) both before and after removal of deep gray-matter connections allowed us to distinguish direct corticocortical connections from those that pass through deep gray matter.

Direct corticocortical connectivity accounted for the majority of connections in dorsal medial cortical regions, and superior parietal cortex at both time points, and additionally in the insula by term (Fig. 4). Difference maps show node degree exclusive of direct corticocortical connections, representing an indirect measure of cortex to deep gray matter to cortex connectivity. Although these connections represent a lower proportion of total connectivity, at 40 wk ∼20% of all connections from the lateral frontal and medial frontal cortices connect to other cortical regions through the deep gray matter.

The proportion of all core and feeder connections that were exclusively corticocortical did not significantly alter during the preterm period [$F_{(1,99)} = 0.42, 0.001$, $P = 0.52, 0.98$, respectively]. However, at the 30-wk time point, despite fewer connections in total, a significantly greater proportion of local connections were exclusively corticocortical [$F_{(1,99)} = 18.07$, $P < 0.001$]. By 40 wk, although there was no significant difference in the total number of core or feeder connections between groups, the proportion of direct corticocortical connections was significantly greater in preterm infants [$F_{(1,99)} = 7.40, 8.02$, respectively, $P < 0.01$ both].

## Discussion

A rich-club network of densely connected cortical hubs is established before the time of normal birth. Rich-club regions include dorsal, medial frontal, and parietal cortex, precuneus, hippocampus, and insula, emulating the highly ordered organization previously described in adults (6). During the third trimester, the number of connections between rich-club regions and the rest of the cortex increases significantly, compatible with the development of the rich club as a communications spine for information transfer across the cerebral network. Network organization is also significantly influenced by the environmental stress of premature extrauterine life, with notable alterations in deep gray matter connectivity compatible with previous studies of thalamocortical connections in preterm populations (23, 24) that result in a greater proportion of direct corticocortical connections compared with healthy term-born infants.

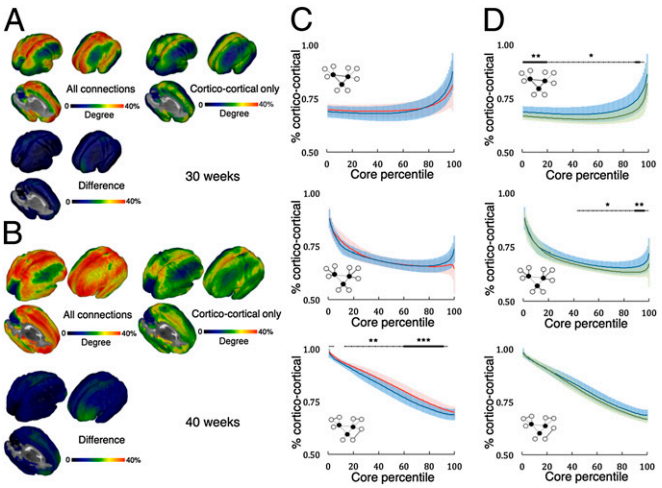


**Fig. 4.** Corticocortical connectivity in the rich club. (*A* and *B*) Group mean maps of normalized node degree for subjects scanned at the 30 wk (*A*; $n = 28$) and 40 wk (*B*; $n = 63$). Degree was calculated before (*Upper Left*) and after (*Upper Right*) excluding streamlines passing through deep gray matter. (*Lower Left*) Difference maps. (*C*) Average core node degree when considering only corticocortical connections as a proportion of node degree when all connections are considered. Core connections (*Top*), feeder connections (*Middle*), and local connections (*Bottom*) are shown separately. Solid lines represent group mean at the early (red) and term (blue) time points (shading represents SD). Post hoc paired *t* tests at each core level were performed when a main effect of age was found; significant differences are shown with dashed (**$P < 0.01$) and solid (***$P < 0.001$) black lines. (*D*) Comparison of corticocortical connectivity data for all infants scanned at term (blue: preterm at term, $n = 46$; green: term controls, $n = 17$). Significant differences are shown with dashed (*$P < 0.05$) and solid (**$P < 0.01$) black lines.

Rich-club organization is a property common to complex networks across many domains (7) and is hypothesized as a basis for efficient global information transfer in the brain (21). Rich clubs are found in the mammalian brain and in the neural circuitry of *Caenorhabditis elegans*, where rich-club neurons are among the first to develop, suggesting that rich-club organization reflects a common and scale-invariant property of neuronal networks (10, 25). In the adult human brain, the rich club is formed by dense, long-distance connections linking cortical hub regions of functional specialization; a configuration that results in increased metabolic demands compared with surrounding non–rich-club regions (6, 26), a high cost that may be offset by the functional benefits of efficient information flow (27).

Few studies have examined whole-brain structural connectivity in the newborn brain to date (12, 15, 28). In contrast to previous reports that intermodular connectivity is relatively sparse in the newborn brain, we report that anatomically segregated cortical hubs are densely connected. We show that the connections between rich-club nodes are significantly longer than between nonrich nodes, and we demonstrate that the developmental window between 30 and 40 wk gestation represents an important period for the establishment of connections between hub regions and the rest of the cortex.

The presence of highly connected cortical hubs is a prominent feature of functional and structural brain networks in adulthood and infancy (3–5, 29). Frontoparietal connectivity in particular is heavily implicated in effective network communication and function (30, 31). Long-distance corticocortical connections are established in the second and third trimester (32) and GAP-43 expression, a marker of axonal growth and elongation, is maximal in cerebral white matter from 21 to 43 wk gestation (33). Histologically, from ~17 wk, the cingulum bundle can be observed connecting frontal and parietal regions (34) and high-resolution, postmortem fetal diffusion tensor imaging has recorded the emergence of short-range corticocortical connections and the eventual formation of an adult-like pattern of corticocortical connectivity by term (35). Following birth, synaptic remodeling is largely dependent on neuronal activity (36), and this process continues throughout childhood (37); however, the pattern of projections remains relatively constant with axonal removal having a limited effect on connectivity at a macroscopic scale (38).

Together, this evidence suggests that much of the macrostructural architecture required for normal brain function is present by the time of normal birth. In particular, the major pathways underlying rich-club organization in the brain are established before 30 wk of gestation. Rich-club connectivity increased predominantly in frontal and parietal regions between 30 and 40 wk following a well-established developmental trajectory for white matter development (39). We have previously found that cortical maturation, indexed by microstructural diffusivity, occurs in tandem in these regions across a similar timeframe (40), and more recent data has shown that disruptions to cortical and underlying white matter development occur in parallel (41); this supports evidence that white matter connectivity and cortical maturation are intrinsically linked (42) and suggests that the establishment of structural connectivity has implications for subsequent functional maturation of cortical hubs. However, this finding presents an intriguing discrepancy between the well-established rich-club network and the functional competencies of the minimally conscious infant brain (43). Recent studies have demonstrated a generally positive correlation between the two modalities, but not a predictive relationship, because many functional configurations can arise from a single structural connectivity pattern (44–46). Our own findings suggest that a relatively complete functional network structure is present by term-equivalent age (16); others have suggested that distinct temporal dynamics in primary sensory and higher-order cortical functional networks in the newborn brain reflect a maturational gradient that appears to align with cortical development (40, 47, 48). Though the significance of these findings is not clear, they demonstrate that functional maturation is a dynamic developmental process (49). We propose that early rich-club organization facilitates this process, providing a foundation for well-formed, if not fully functional, structural networks.

Preterm birth is associated with altered brain development, characterized by microstructural white matter and cortical alterations and selective tissue loss in the deep gray matter, and confers a significant risk for poor neurodevelopmental outcome (24, 50, 51). Stressors associated with neonatal intensive care, including respiratory management, social isolation, and nutrition, can also impact negatively on brain development (52–54). Our data suggest that exposure to the extrauterine environment following preterm birth subtly alters the macrostructural development of the whole-brain structural connectome during the third trimester by reducing the network capacity of the deep gray matter. Although rich-club organization remained intact, there was evidence of a significant increase in short-range connectivity between peripheral nodes in the lateral frontal and parietal cortex. In addition, removing streamlines through the deep gray matter revealed a significant increase in direct corticocortical connectivity (and a subsequent reduction in the proportion of rich-club connections passing through the deep gray matter) in preterm infants. Notably, the proportion of direct corticocortical connections from rich-club nodes did not change between 30 and 40 wk in the preterm cohort, suggesting a disruption of normal network development following premature birth.

Although the clinical significance of these disruptions is not yet known, prematurity is associated with higher rates of neurodevelopmental disorders, such as attention deficit hyperactivity disorder and autism, which have both been recently characterized as disorders of connectivity (55, 56). A consensus has not been reached on the nature of the network disturbances underlying these disorders, but we speculate that structural disruptions arising from changes secondary to the early emergence

of rich-club organization, such as the increases in local cortical–cortical connectivity observed in the present study, may represent possible candidate features. The presence and state of rich-club organization in these clinical populations therefore warrants further investigation.

Anatomical dissections have revealed that a substantial proportion of frontoparietal connections are formed by short-association U fibers (57), whereas both the frontal and parietal cortices exhibit extensive, direct, high-capacity projections to the striatum and thalamus (58, 59). Given that the roles of parallel and distributed frontal–striatal–thalamic circuits in higher-order cognitive functions are well est ablished (60), it is also of note that connectivity of the lateral frontal cortex appeared to be most dependent on connections passing through the deep gray matter by term-equivalent age; this suggests that alterations to frontal–subcortical connectivity may limit communication efficiency between hubs within the rich club with a potential impact on subsequent neurocognitive development. Whether the significant increase in corticocortical connectivity between peripheral nodes reflects exuberant corticocortical connectivity via short U fibers in preterm neonates remains unclear, and further investigation is needed. The combination of advanced diffusion modeling techniques (i.e., spherical deconvolution) (61, 62) and high-resolution tracing of corticocortical fibers will enable the targeted exploration of corticocortical connectivity in this population, and appropriate acquisition protocols for neonates are currently under active research (63).

Our observations are limited by the resolution available to whole-brain diffusion MRI, and by the relatively coarse nature of tractography-based connectomics, but it is proposed that postnatal development of neurocognitive functions is dependent on the fine-tuning of synapses and short-range fibers with limited remodeling of the fundamental structural architecture. With advances in microstructural modeling of the developing cortex (40) and the development of methods to combine functional and structural connectivity information (44, 46), these data will provide insights into human brain development and dysfunction.

## Materials and Methods

Ethical permission for this study was granted by the local Research Ethics Committees (the City and East London Research Ethics Committee; the Hammersmith, Queen Charlotte's and Chelsea Research Ethics Committee). Written parental consent was obtained for each infant.

**Subjects.** Forty-six preterm-born infants [22 male; median (range) gestational age at birth $27^{+1}$ ($24^{+4}$–$34^{+5}$) weeks; median birth weight 0.97 (0.62–2.02) kg] were scanned at term-equivalent age [median postmenstrual age $41^{+0}$ ($38^{+0}$–$44^{+1}$) weeks]. A subset of 28 (14 males, median gestational age $27^{+2}$) were also scanned at an earlier time point during the preterm period [median age $31^{+1}$ ($25^{+2}$–$33^{+0}$) weeks]. See *SI Materials and Methods* and Table S2 for details.

Seventeen healthy term-born control infants were also examined [six male; median (range) gestational age at birth $38^{+6}$ ($36^{+0}$–$41^{+6}$) weeks; median postmenstrual age at scan $41^{+4}$ ($39^{+0}$–$44^{+4}$) weeks; median birth weight 3.12 (2.68–4.20) kg].

**Imaging.** Each infant successfully underwent T2-weighted MRI and 32-direction diffusion MRI acquisition. MRI was performed on a Philips 3-Tesla system (Philips Medical Systems) within the neonatal intensive care unit using an eight-channel phased-array head coil (see *SI Materials and Methods* for details).

**Whole-Brain Connectivity.** For each infant, a cortical mask was derived from tissue segmentation driven by age-specific priors (64). Cortical masks were inspected slice-by-slice and manually edited to remove any remaining noncortical voxels.

Poisson disk sampling was used to parcellate each cortical mask into ~500 ROIs (mean ± SD = 499.5 ± 6.1) as described previously (23). This process produces a set of randomly distributed and similarly sized cortical ROI and does not rely upon atlas-based anatomical borders or landmarks but results in different cortical ROI across individuals, precluding direct comparison; to address this, we adopted a sampling procedure in which 100 sets of random cortical ROI were produced for each infant, and whole-brain tractography was repeated for each set to generate 100 networks per subject. Topological metrics and nodal connectivity maps derived from each network were then combined to provide summary measures and to generate voxel-wise connectivity maps that allow concatenation and comparison across subjects (Fig. S1).

All sets of cortical ROI were transformed from T2 space into diffusion space using nonrigid registration as implemented in the IRTK software package (65). Before processing, all datasets were visually assessed for motion artifacts (*SI Materials and Methods*). Diffusion data were preprocessed using FSL's Diffusion Toolkit (www.fmrib.ox.ac.uk/fsl/). For each set of cortical target regions, 1,000 streamlines were propagated per seed voxel using a modified version of ProbtrackX (66, 67), tracking stopped when streamlines reached a target region, left the brain mask, or entered voxels containing cerebrospinal fluid. Although deep gray-matter structures were not included as targets during tractography, streamlines passing through them to connect two cortical targets were included in the initial network analysis.

**Network Construction and Analysis.** A connection matrix was constructed from each of the 100 sets of cortical ROI for each subject (*SI Materials and Methods* and Fig. S1). The Brain Connectivity Toolbox (68), implemented in MatLab (MathWorks, Inc.), was used for network analysis. Edge density, clustering coefficient, $C$, and characteristic path length, $L$, were averaged over all nodes in each network and the mean over 100 networks taken as a summary measure per subject (Fig. S1*D*). Normalized $L$ and $C$ metrics were estimated by comparing each network to a set of randomized networks ($n$ = 100 per graph, $n$ = 10,000 per subject) with equivalent size and degree distribution (69).

**Rich-Club Organization.** For a $N \times N$ matrix $M$, where $N$ equals the number of ROI in a parcellation, a measure for rich-club organization can be calculated over a range of degrees $k$:

$$\phi(k) = \frac{2E_{>k}}{N_{>k}(N_{>k}-1)},$$

where, after removing all nodes $N$ with degree less than $k$, the rich-club coefficient $\phi(k)$ equals the ratio of connections present between the remaining nodes $E_{>k}$ and the total number of possible connections that would be present if the remaining nodes were fully connected (6, 7). For comparison across individuals, $\phi(k)$ is typically normalized by the average coefficient calculated over a set of random networks $\phi_{\text{random}}(k)$. A normalized rich-club coefficient $\phi_{\text{norm}}$ of >1 across a range of $k$ indicates rich-club organization in the network (Fig. S1*B*). Because $\phi$ varies as a function of degree $k$, a threshold is often applied to designate a discrete set of high-degree nodes for which $\phi$ and $\phi_{\text{norm}}$ are calculated (6). In this study, to allow for comparison across networks with varying node number and degree, nodes were labeled as belonging to a network core or periphery based on their respective degree. All nodes were ranked according to degree, and nodes with the lowest number of connections removed in one-percentile increments (approximately five nodes at a time); excluded nodes were designated as peripheral, with the remaining nodes forming the network core. $\phi$ and $\phi_{\text{norm}}$ were then calculated for each network core, as lower degree nodes were incrementally removed; this allows for comparison between core networks of equal size in each group.

**Subject Comparison.** To visualize and compare nodal metrics, a recently developed technique—gray matter-based spatial statistics—was used to project connectivity data onto a skeletonized representation of group mean cortical anatomy to mitigate the effects of misalignment from registration, intersubject variability, and partial volume contamination (40).

**ACKNOWLEDGMENTS.** Support for this work was provided from the Medical Research Council, Engineering and Physical Sciences Research Council, National Institute for Health Research Comprehensive Biomedical Research Centre awards to Guy's and St Thomas' National Health Service Foundation Trust in partnership with King's College London and King's College Hospital NHS Foundation Trust, and the Garfield Weston Foundation.

1. Felleman DJ, Van Essen DC (1991) Distributed hierarchical processing in the primate cerebral cortex. *Cereb Cortex* 1(1):1–47.

2. Markov NT, et al. (2013) The role of long-range connections on the specificity of the macaque interareal cortical network. *Proc Natl Acad Sci USA* 110(13):5187–5192.

3. Sporns O, Honey CJ, Kötter R (2007) Identification and classification of hubs in brain networks. *PLoS ONE* 2(10):e1049.
4. Buckner RL, et al. (2009) Cortical hubs revealed by intrinsic functional connectivity: Mapping, assessment of stability, and relation to Alzheimer's disease. *J Neurosci* 29(6): 1860–1873.
5. Power JD, Schlaggar BL, Lessov-Schlaggar CN, Petersen SE (2013) Evidence for hubs in human functional brain networks. *Neuron* 79(4):798–813.
6. van den Heuvel MP, Sporns O (2011) Rich-club organization of the human connectome. *J Neurosci* 31(44):15775–15786.
7. Colizza V, Flammini A, Serrano MA, Vespignani A (2006) Detecting rich-club ordering in complex networks. *Nat Phys* 2(2):110–115.
8. Xu X-K, Zhang J, Small M (2010) Rich-club connectivity dominates assortativity and transitivity of complex networks. *Phys Rev E Stat Nonlin Soft Matter Phys* 82(4 Pt 2): 046117.
9. Gómez-Gardeñes J, Zamora-López G, Moreno Y, Arenas A (2010) From modular to centralized organization of synchronization in functional areas of the cat cerebral cortex. *PLoS ONE* 5(8):e12313.
10. Harriger L, van den Heuvel MP, Sporns O (2012) Rich club organization of macaque cerebral cortex and its role in network communication. *PLoS ONE* 7(9):e46497.
11. Hagmann P, et al. (2010) White matter maturation reshapes structural connectivity in the late developing human brain. *Proc Natl Acad Sci USA* 107(44):19067–19072.
12. Yap P-T, et al. (2011) Development trends of white matter connectivity in the first years of life. *PLoS ONE* 6(9):e24678.
13. LaMantia AS, Rakic P (1990) Axon overproduction and elimination in the corpus callosum of the developing rhesus monkey. *J Neurosci* 10(7):2156–2175.
14. Price DJ, Blakemore C (1985) Regressive events in the postnatal development of association projections in the visual cortex. *Nature* 316(6030):721–724.
15. Tymofiyeva O, et al. (2013) A DTI-based template-free cortical connectome study of brain maturation. *PLoS ONE* 8(5):e63310.
16. Doria V, et al. (2010) Emergence of resting state networks in the preterm human brain. *Proc Natl Acad Sci USA* 107(46):20015–20020.
17. Fransson P, et al. (2007) Resting-state networks in the infant brain. *Proc Natl Acad Sci USA* 104(39):15531–15536.
18. Amaral LA, Scala A, Barthelemy M, Stanley HE (2000) Classes of small-world networks. *Proc Natl Acad Sci USA* 97(21):11149–11152.
19. Achard S, Salvador R, Whitcher B, Suckling J, Bullmore E (2006) A resilient, low-frequency, small-world human brain functional network with highly connected association cortical hubs. *J Neurosci* 26(1):63–72.
20. Shi F, et al. (2011) Infant brain atlases from neonates to 1- and 2-year-olds. *PLoS ONE* 6(4):e18746.
21. van den Heuvel MP, Kahn RS, Goñi J, Sporns O (2012) High-cost, high-capacity backbone for global brain communication. *Proc Natl Acad Sci USA* 109(28): 11372–11377.
22. Smith SM, Nichols TE (2009) Threshold-free cluster enhancement: Addressing problems of smoothing, threshold dependence and localisation in cluster inference. *Neuroimage* 44(1):83–98.
23. Ball G, et al. (2013) The influence of preterm birth on the developing thalamocortical connectome. *Cortex* 49(6):1711–1721.
24. Ball G, et al. (2012) The effect of preterm birth on thalamic and cortical development. *Cereb Cortex* 22(5):1016–1024.
25. Towlson EK, Vértes PE, Ahnert SE, Schafer WR, Bullmore ET (2013) The rich club of the *C. elegans* neuronal connectome. *J Neurosci* 33(15):6380–6387.
26. Collin G, Sporns O, Mandl RCW, van den Heuvel MP (2013) Structural and functional aspects relating to cost and benefit of rich club organization in the human cerebral cortex. *Cereb Cortex*, 10.1093/cercor/bht064.
27. Bullmore E, Sporns O (2012) The economy of brain network organization. *Nat Rev Neurosci* 13(5):336–349.
28. Ratnarajah N, et al. (2013) Structural connectivity asymmetry in the neonatal brain. *Neuroimage* 75:187–194.
29. Pandit AS, et al. (2013) Whole-brain mapping of structural connectivity in infants reveals altered connection strength associated with growth and preterm birth. *Cereb Cortex*, 10.1093/cercor/bht086.
30. He BJ, et al. (2007) Breakdown of functional connectivity in frontoparietal networks underlies behavioral deficits in spatial neglect. *Neuron* 53(6):905–918.
31. Wang L, et al. (2010) Effective connectivity of the fronto-parietal network during attentional control. *J Cogn Neurosci* 22(3):543–553.
32. Kostović I, Jovanov-Milosević N (2006) The development of cerebral connections during the first 20-45 weeks' gestation. *Semin Fetal Neonatal Med* 11(6):415–422.
33. Haynes RL, et al. (2005) Axonal development in the cerebral white matter of the human fetus and infant. *J Comp Neurol* 484(2):156–167.
34. Vasung L, et al. (2010) Development of axonal pathways in the human fetal fronto-limbic brain: Histochemical characterization and diffusion tensor imaging. *J Anat* 217(4):400–417.
35. Takahashi E, Folkerth RD, Galaburda AM, Grant PE (2012) Emerging cerebral connectivity in the human fetal brain: An MR tractography study. *Cereb Cortex* 22(2): 455–464.
36. Peng Y-R, et al. (2009) Coordinated changes in dendritic arborization and synaptic strength during neural circuit development. *Neuron* 61(1):71–84.
37. Bourgeois JP, Rakic P (1993) Changes of synaptic density in the primary visual cortex of the macaque monkey from fetal to adult stage. *J Neurosci* 13(7):2801–2820.
38. Innocenti GM, Price DJ (2005) Exuberance in the development of cortical networks. *Nat Rev Neurosci* 6(12):955–965.
39. Kinney HC, Brody BA, Kloman AS, Gilles FH (1988) Sequence of central nervous system myelination in human infancy. II. Patterns of myelination in autopsied infants. *J Neuropathol Exp Neurol* 47(3):217–234.
40. Ball G, et al. (2013) Development of cortical microstructure in the preterm human brain. *Proc Natl Acad Sci USA* 110(23):9541–9546.
41. Melbourne A, et al. (2014) Preterm birth affects the developmental synergy between cortical folding and cortical connectivity observed on multimodal MRI. *Neuroimage* 89:23–34.
42. Van Essen DC (1997) A tension-based theory of morphogenesis and compact wiring in the central nervous system. *Nature* 385(6614):313–318.
43. Lagercrantz H, Changeux J-P (2009) The emergence of human consciousness: From fetal to neonatal life. *Pediatr Res* 65(3):255–260.
44. Honey CJ, et al. (2009) Predicting human resting-state functional connectivity from structural connectivity. *Proc Natl Acad Sci USA* 106(6):2035–2040.
45. van den Heuvel MP, Mandl RCW, Kahn RS, Hulshoff Pol HE (2009) Functionally linked resting-state networks reflect the underlying structural connectivity architecture of the human brain. *Hum Brain Mapp* 30(10):3127–3141.
46. Deligianni F, et al. (2011) A probabilistic framework to infer brain functional connectivity from anatomical connections. *Inf Process Med Imaging* 22:296–307.
47. Fransson P, et al. (2013) Early development of spatial patterns of power-law frequency scaling in FMRI resting-state and EEG data in the newborn brain. *Cereb Cortex* 23(3):638–646.
48. Fransson P, Åden U, Blennow M, Lagercrantz H (2011) The functional architecture of the infant brain as revealed by resting-state fMRI. *Cereb Cortex* 21(1):145–154.
49. Dosenbach NUF, et al. (2010) Prediction of individual brain maturity using fMRI. *Science* 329(5997):1358–1361.
50. Rathbone R, et al. (2011) Perinatal cortical growth and childhood neurocognitive abilities. *Neurology* 77(16):1510–1517.
51. Boardman JP, et al. (2010) A common neonatal image phenotype predicts adverse neurodevelopmental outcome in children born preterm. *Neuroimage* 52(2):409–414.
52. Pineda RG, et al. (2014) Alterations in brain structure and neurodevelopmental outcome in preterm infants hospitalized in different neonatal intensive care unit environments. *J Pediatr* 164(1):52–60.
53. Smith GC, et al. (2011) Neonatal intensive care unit stress is associated with brain development in preterm infants. *Ann Neurol* 70(4):541–549.
54. Morgan C, McGowan P, Herwitker S, Hart AE, Turner MA (2014) Postnatal head growth in preterm infants: A randomized controlled parenteral nutrition study. *Pediatrics* 133(1):e120–e128.
55. Uddin LQ, Supekar K, Menon V (2013) Reconceptualizing functional brain connectivity in autism from a developmental perspective. *Front Hum Neurosci* 7:458.
56. Liston C, Malter Cohen M, Teslovich T, Levenson D, Casey BJ (2011) Atypical prefrontal connectivity in attention-deficit/hyperactivity disorder: Pathway to disease or pathological end point? *Biol Psychiatry* 69(12):1168–1177.
57. Maldonado IL, Mandonnet E, Duffau H (2012) Dorsal fronto-parietal connections of the human brain: A fiber dissection study of their composition and anatomical relationships. *Anat Rec (Hoboken)* 295(2):187–195.
58. Goldman-Rakic PS, Porrino LJ (1985) The primate mediodorsal (MD) nucleus and its projection to the frontal lobe. *J Comp Neurol* 242(4):535–560.
59. Yeterian EH, Pandya DN (1993) Striatal connections of the parietal association cortices in rhesus monkeys. *J Comp Neurol* 332(2):175–197.
60. Cummings JL (1993) Frontal-subcortical circuits and human behavior. *Arch Neurol* 50(8):873–880.
61. Tournier J-D, Calamante F, Connelly A (2007) Robust determination of the fibre orientation distribution in diffusion MRI: Non-negativity constrained super-resolved spherical deconvolution. *Neuroimage* 35(4):1459–1472.
62. Tournier JD, Calamante F, Gadian DG, Connelly A (2004) Direct estimation of the fiber orientation density function from diffusion-weighted MRI data using spherical deconvolution. *Neuroimage* 23(3):1176–1185.
63. Pandit AS, Ball G, Edwards AD, Counsell SJ (2013) Diffusion magnetic resonance imaging in preterm brain injury. *Neuroradiology* 55(Suppl 2):65–95.
64. Serag A, et al. (2012) Construction of a consistent high-definition spatio-temporal atlas of the developing brain using adaptive kernel regression. *Neuroimage* 59(3): 2255–2265.
65. Rueckert D, et al. (1999) Nonrigid registration using free-form deformations: Application to breast MR images. *IEEE Trans Med Imaging* 18(8):712–721.
66. Robinson EC, Hammers A, Ericsson A, Edwards AD, Rueckert D (2010) Identifying population differences in whole-brain structural networks: A machine learning approach. *Neuroimage* 50(3):910–919.
67. Behrens TE, Berg HJ, Jbabdi S, Rushworth MF, Woolrich MW (2007) Probabilistic diffusion tractography with multiple fibre orientations: What can we gain? *Neuroimage* 34(1):144–155.
68. Rubinov M, Sporns O (2010) Complex network measures of brain connectivity: Uses and interpretations. *Neuroimage* 52(3):1059–1069.
69. Maslov S, Sneppen K (2002) Specificity and stability in topology of protein networks. *Science* 296(5569):910–913.